Dynamic Plasmonic Platform To Investigate the Correlation between Far-Field Optical Response and SERS Signal of Analytes

Mai Nguyen, Issam Kherbouche, Macilia Braik, Abderrahmane Belkhir, Leïla Boubekeur-Lecaque, Jean Aubard, Claire Mangeney, Nordin Felidj

ACS OMEGA

Article

Cite This: ACS Omega 2019, 4, 1144−1150

http://pubs.acs.org/journal/acsodf

Dynamic Plasmonic Platform To Investigate the Correlation between Far-Field Optical Response and SERS Signal of Analytes

Mai Nguyen,[†] Issam Kherbouche,[‡,∥] Macilia Braik,[§] Abderrahmane Belkhir,[§] Leïla Boubekeur-Lecaque,[∥] Jean Aubard,[∥] Claire Mangeney,*[,‡] and Nordin Felidj*[,∥]

[†]School of Chemical Engineering, Hanoi University of Science and Technology, 1 Dai Co Viet Road, 10000 Hanoi, Vietnam
[‡]University Paris 05, Lab Chim & Biochim Pharmacolog & Toxicol, UMR 8601, 45 rue des Saints-Pères, 75006 Paris, France
[§]Laboratoire de Physique et Chimie Quantique, Université Mouloud Mammeri, B.P. 17 RP, 15000 Tizi-Ouzou, Algeria
[∥]ITODYS Laboratory, UMR 7086, Université Paris Diderot, 15 rue Jean Antoine de Baïf, 75013 Paris, France

Supporting Information

ABSTRACT: The design of surface-enhanced Raman spectroscopy (SERS) platforms based on the coupling between plasmonic nanostructures and stimuli-responsive polymers has attracted considerable interest over the past decades for the detection of a wide range of analytes, including pollutants and biological molecules. However, the SERS intensity of analytes trapped inside smart hybrid nanoplatforms is subject to important fluctuations because of the spatial and spectral variation of the plasmonic near-field enhancement (i.e., its dependence with the distance to the nanoparticle surface and with the localized surface plasmon resonance). Such fluctuations may impair interpretation and quantification in sensing devices. In this paper, we investigate the influence of the plasmonic near-field profile upon the Raman signal intensity of analytes trapped inside thermoresponsive polymer-coated gold nanoarrays. For this, well-defined plasmonic arrays (nanosquares and nanocylinders) were modified by poly(*N*-isopropylacrylamide) (PNIPAM) brushes using surface-initiated atom-transfer radical polymerization. Molecular probes were trapped inside these Au@PNIPAM nanostructures by simple physisorption or by covalent grafting at the end of PNIPAM brushes, using click chemistry. The SERS spectra of molecular probes were studied along various heating/cooling cycles, demonstrating a strong correlation between SERS intensities and near-field spectral profile of underlying nanoparticles, as confirmed by simulations based on the finite difference time domain method. Thermoresponsive plasmonic devices thus provide an ideal dynamic SERS platform to investigate the influence of the near-field plasmonic profile upon the SERS response of analytes.

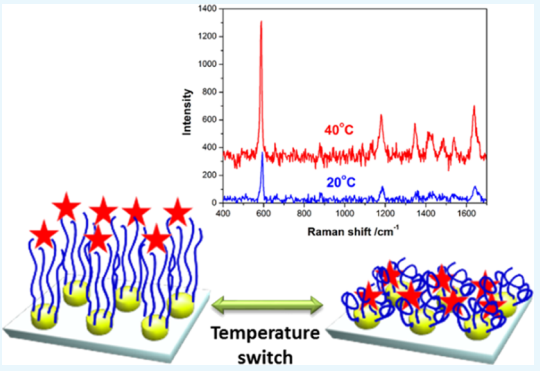

1. INTRODUCTION

Surface-enhanced Raman spectroscopy (SERS) has gained popularity over the past decades, owing to its ability to detect and identify a large variety of compounds with single-molecule sensitivity.[1−4] SERS inherits the rich chemical fingerprint information from Raman spectroscopy and gains sensitivity through the amplification of electromagnetic fields generated by the excitation of metallic nanoparticles (NPs) localized surface plasmon (LSP).[5−8] This optical effect results from collective oscillations of the conductive electrons at the particle surface and is characterized by a strong extinction in the visible and near-infrared spectral regions.[9] In the near field, LSP excitation leads to huge local electric fields in the vicinity of the nanostructures.[10] As a result, when a molecule displaying a high surface affinity is located in the immediate vicinity of NPs (distance < 5 nm), its Raman signal can be strongly amplified and intense SERS spectra can be collected.[11−15] In contrast, the near-field effect vanishes progressively when the analytes are located further away from the surface (distance > 5−10 nm). It is therefore a challenge to probe analytes with a small surface affinity. To tackle this issue and concentrate the target analytes near the NP surface, novel surface chemistries have been proposed, relying on thiol-based chemoreceptors[16] or molecularly imprinted polymers.[17] Another attractive means to trap molecules in the vicinity of plasmonic NPs is to cover them by stimuli-responsive polymers, that is, polymers which undergo large physical or chemical changes in response to small external changes in their environment (such as variations of temperature, pH, ionic strength, ...).[5,18−22] The polymer shell either swells or collapses when responding to the external stimuli. This change in volume was utilized as a means to trap analytes and get them close to the metal core, where the electromagnetic field is significantly enhanced, even in the case of analytes displaying a low affinity toward the metal surface.

Received: November 7, 2018
Accepted: January 2, 2019
Published: January 14, 2019

DOI: 10.1021/acsomega.8b03107
ACS Omega 2019, 4, 1144−1150

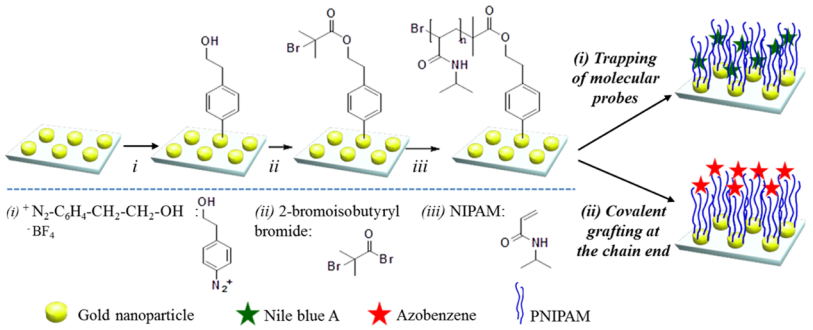

Figure 1. Representative scheme of the two strategies to investigate the SERS intensity fluctuations of two molecular probes (NBA and AB) as a function of the near-field plasmonic response: (i) unspecific trapping of NBA molecular probes inside the whole PNIPAM brushes by simple physisorption and (ii) covalent grafting of AB at the end of PNIPAM brushes, using click chemistry.

Such stimuli-responsive plasmonic nanostructures have been demonstrated to be ideal systems for the detection of a wide range of analytes, including pollutants[18] and biological molecules.[23] The huge SERS enhancement obtained upon LSP excitation ensures a high sensitivity, allowing acquiring the characteristic fingerprint of any kind of target molecules even at low concentrations. However, considering the spatial and spectral profile of plasmonic near-field enhancement, the SERS intensities of analytes trapped inside stimuli-responsive polymers are subject to important variations depending on their distance from the NP surface, which could impair interpretation and quantification in sensing devices. To date, considerable efforts have been made to improve the sensitivity of SERS analysis using metal NP substrates with different shapes, dimensions, and stimuli-responsive polymers. However, to our knowledge, there is no study about the Raman intensity fluctuations due to spatial and spectral variations of the plasmonic near-field profile of the underlying nanostructures, when the distance from the NP surface is dynamically modified through an external stimulus.

In this work, we tackle this issue by investigating the influence of the spatial and spectral profile of the plasmonic near-field enhancement upon the Raman signal intensity of analytes trapped inside thermoresponsive brushes, here poly-*N*-isopropylacrylamide (PNIPAM). PNIPAM was chosen as it is a widely known polymer for its lower critical solution temperature (LCST) phenomenon with a sharp cloud point ranging from 31 to 33 °C in water.[24,25] Below the LCST, PNIPAM brushes exist as coils because of hydrogen bonding of amide groups with water, whereas above the LCST, the polymer conformation changes from hydrophilic linear and flexible PNIPAM chains to hydrophobic collapsed globules. These temperature-dependent conformational changes were used to trap analytes in aqueous solutions and record their SERS spectra. Nile blue A (NBA) and azobenzene (AB) were chosen as molecular probes because of their well-known Raman signature. The experiments were performed on well-defined and highly uniform plasmonic arrays, obtained by electron beam lithography (EBL), allowing systematic SERS studies. PNIPAM brushes were attached on plasmonic arrays via a combination of diazonium salt chemistry and surface-initiated atom-transfer radical polymerization (SI-ATRP), providing a perfect control over polymer thickness. Two strategies (illustrated in Figure 1) were used to investigate the analyte SERS intensity fluctuations as a function of the near-field plasmonic response: (i) the unspecific trapping of molecular probes inside the whole PNIPAM brushes by simple physisorption and (ii) their covalent grafting at the end of PNIPAM brushes, using click chemistry. The thermoresponsive plasmonic devices developed in this paper thus provide an ideal dynamic SERS platform to investigate the influence of the near-field plasmonic profile upon the SERS response of analytes.

2. RESULTS AND DISCUSSION

Regular arrays of gold NPs (nanosquares and nanocylinders) deposited on indium tin oxide substrates were elaborated by EBL and functionalized by PNIPAM brushes, leading to Au@PNIPAM samples. The functionalization strategy (see details in the Supporting Information) included two major steps: (i) the spontaneous grafting of initiators derived from diazonium salts on gold NPs and (ii) the grafting of PNIPAM chains from the surface via SI-ATRP. Typical AFM images of the gold NP arrays before and after PNIPAM grafting are displayed in Figures 2 and S2. The dry PNIPAM thickness, measured from

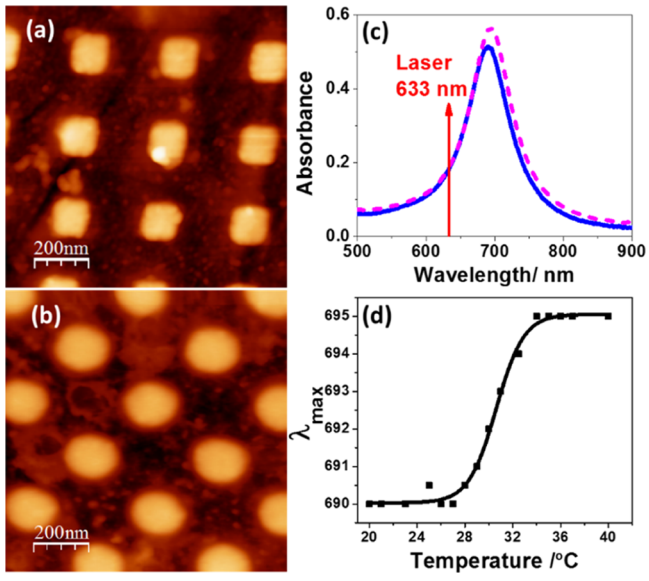

Figure 2. Characteristic of Au@PNIPAM nanostructures. (a,b) AFM images recorded in air at room temperature of PNIPAM-coated gold nanosquares (a) and nanocylinders (b). (c) Extinction spectra of nanosquare Au@PNIPAM, recorded in water at 20 °C (blue spectrum) and 40 °C (pink dashed spectrum); the vertical red line indicates the wavelength of laser excitation (at 633 nm), which has been used later for the SERS experiments. (d) Evolution of the LSP wavelength (λ_{max}) vs temperature for nanosquare Au@PNIPAM.

DOI: 10.1021/acsomega.8b03107
ACS Omega 2019, 4, 1144−1150

AFM images, was $h_{dry} \approx 5 \pm 2$ nm. Relying on a previous report, the swelling ratio of PNIPAM brushes, defined as $\alpha = h_{swollen}/h_{dry}$ (where $h_{swollen}$ and h_{dry} correspond to the swollen and dry brush thickness, respectively), is approximately $\alpha \approx 2$.[27] Therefore, the thickness of swollen PNIPAM brushes in water at $T < T_{LCST}$ could be estimated to be ~10 ± 2 nm. The extinction spectra of nanosquare Au@PNIPAM in water at 20 °C (below the LCST), displayed in Figure 2, showed an intense localized surface plasmon resonance (LSPR) band at 690 nm, which slightly shifted to 695 nm at 40 °C (above the LCST) (see Figure 2). This red shift is attributed to the collapse of polymer brushes above the LCST, leading to an increase of both the polymer density close to the NPs and the refractive index of the surrounding medium.

The temperature dependence of the LSP wavelength, displayed in Figure 2d, evidences a sharp transition around 32 °C, revealing the two conformational regimes of polymer brushes (swollen and collapsed), as previously reported.[28] Temperature-dependent SERS experiments were then performed on Au@PNIPAM using NBA as a molecular probe. For this, the Au@PNIPAM substrates were first immersed in an NBA aqueous solution (at 1 nM) for 5 min and rinsed in water and ethanol. The SERS experiments were carried out in water upon heating from 20 to 40 °C with a 633 nm laser excitation, blue-shifted with respect to the maximum of the LSPR of the plasmonic structures. Figure 3 shows the SERS spectra recorded on nanosquare and nanocylinder Au@PNIPAM in water at 20 and 40 °C. The Raman bands (gathered in Table 1) are assigned to ring-stretching vibrations at 1639, 1542, 1493, 1433, 1419, and 1350 cm^{-1}, C−H bending at 1256 and 1185 cm^{-1}, C−C−C and N−C−C in-plane bending at 664 cm^{-1}, and C−C−C and C−N−C deformations at 592 and 499 cm^{-1}.

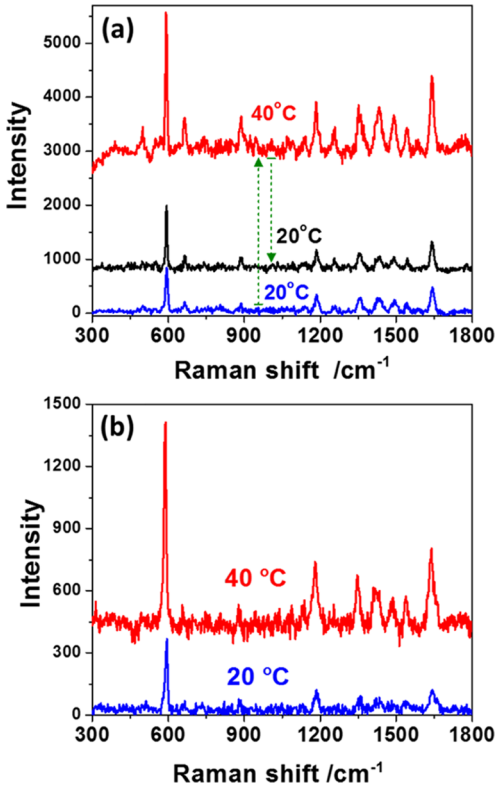

Figure 3. SERS response vs temperature for NBA probes trapped in Au@PNIPAM. (a) SERS spectra recorded on nanosquare Au@PNIPAM at 20 °C (blue spectrum) and 40 °C (red spectrum) and back to 20 °C (black spectrum); (b) SERS spectra recorded on nanocylinder Au@PNIPAM at 20 °C (blue spectrum) and 40 °C (red spectrum). The samples were excited with a 633 nm laser line (power 6.8 μW) and an acquisition time of 1s. For the sake of clarity, the SERS spectra were vertically shifted.

These assignments are in good agreement with the Raman signature of NBA reported in the literature.[29] Note that although the Raman peaks of the aryl film are observed in the absence of NBA molecules (see Figure S8), its signature is completely hidden in the presence of NBA. Remarkably, the intensity of all NBA Raman bands was observed to increase progressively with the temperature as shown in Figure 4, reaching an ~3-fold increase at 40 °C, compared to 20 °C. Reversibly, cooling down from 40 to 20 °C leads to a decrease of the SERS signal almost back to its original intensity, as illustrated in Figure 4b with the reversible increase/decrease of the 1186 cm^{-1} band versus temperature. These results emphasize the strong and reversible SERS response of Au@PNIPAM nanostructures to the external temperature switch.

These variations in the SERS signals of NBA probes with temperature can be interpreted as follows: when the PNIPAM brushes collapse above LCST, the analytes are trapped in the vicinity of the NP surface where the local fields are strongly enhanced, resulting in intense SERS spectra. In contrast, below the LCST, NBA molecules are randomly distributed inside the swollen PNIPAM brushes and are thus located further from the surface where the near-field enhancement vanishes. This "on/off" switching of near-field enhancement depending on the distance between the molecular probe and the NP surface was modeled using the finite difference time domain (FDTD) method. In the calculations, we considered a square array of square particles (side: 100 nm, height: 40 nm, interparticle distance: 300 nm) displaying a LSPR in water of around 720 nm, as shown in Figure 5.

The structure was illuminated at normal incidence along the *z*-axis from the glass (see Figure S7). From the calculation, it is clear that the electric field intensity is maximum ("on" configuration) when the excitation matches the LSP at λ_{max} and decreases rapidly away from the NP surface. When the excitation is not exactly at λ_{max}, for example, here at wavelengths corresponding to the half-height of the maximum (700 or 740 nm), the electric field intensity is slightly lower but also decreases away from the NP surface. Above 5−6 nm, the intensities of the electric field calculated at 700, 720, and 740 nm are similar with low values and become close to zero beyond 10 nm ("off" configuration). Therefore, when the molecular probes are located less than 5 nm from the NP surface, it is expected that their Raman peak intensities are influenced by the local field spectral profile of the LSPR. In contrast, above 10 nm, the Raman peak intensities should follow that of normal Raman spectra. To demonstrate this assumption, the ratio $I_{40°C/20°C}$ (where $I_{40°C}$ and $I_{20°C}$ correspond to the Raman intensities at 40 and 20 °C, respectively) of various Raman bands was calculated and plotted versus their peak frequency (see Figure 6).

The Raman peak intensity at 40 °C, above the LCST, reflects the "on" configuration where molecular probes are located inside the electric field enhancement region. On the contrary, the Raman peak intensity at 20 °C, below the LCST, reflects the "off" configuration, where the molecular probes are located outside the intense electric field region. In Figure 6, the

DOI: 10.1021/acsomega.8b03107
ACS Omega 2019, 4, 1144−1150

Table 1. Wavenumber σ_R and Wavelength λ_R of the Various Raman Bands Denoted from (1) to (8)

Raman band	(1)	(2)	(3)	(4)	(5)	(6)	(7)	(8)
σ_R (cm^{-1})	499	592	664	888	1185	1350	1433	1639
λ_R (nm)	654	658	661	671	684	692	696	706

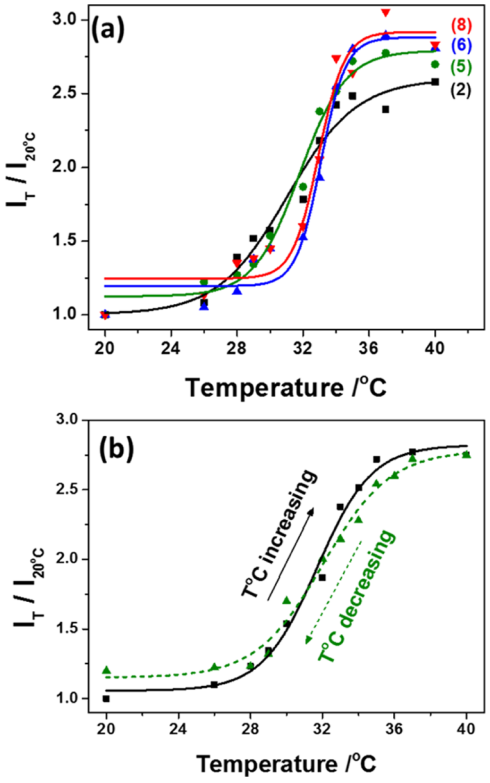

Figure 4. (a) Temperature dependence of $I_T/I_{20°C}$ (where I_T and $I_{20°C}$ correspond to the Raman intensity at the temperature T and at 20 °C, respectively) for the Raman bands at (2) 592; (5) 1185; (6) 1350; and (8) 1639 cm^{-1}. (b) Reversible intensity ratio variation of the Raman band at 1181 cm^{-1} with temperature increase/decrease.

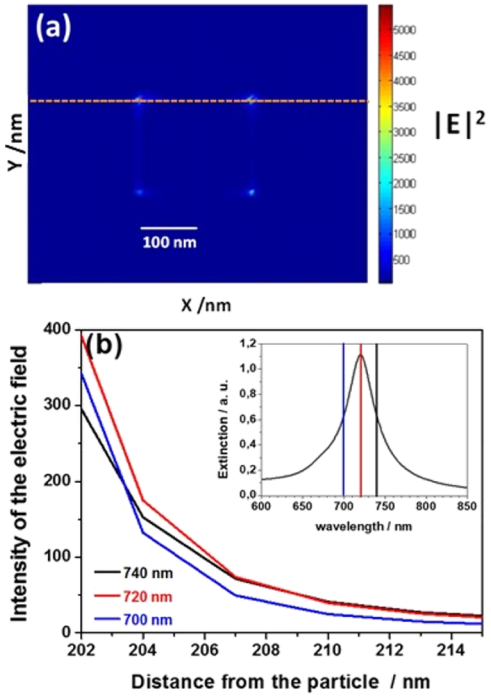

Figure 5. (a) 2D mapping of the intensity of the electric field of a square gold particle (side: 100 nm, height: 40 nm, interparticle distance: 300 nm), calculated at the maximum of the LSP band (720 nm). The dashed line in (a) corresponds to the selected direction used to plot the intensity vs the distance. (b) FDTD simulation of the intensity of the electric field vs the distance to the particle surface. Calculations are provided at maximum of the LSPR (720 nm) and at wavelengths corresponding to the half-height (700 and 740 nm). Inset: Calculated extinction spectrum.

evolution $I_{40°C/20°C} = f(\lambda)$ was compared with the profile of the extinction spectrum of Au@PNIPAM. From this curve, it is clear that the higher $I_{40°C/20°C}$ values are obtained when the frequency of a particular Raman peak is close to the LSP frequency. Generally, a remarkable correlation between the ratio $I_{40°C/20°C}$ for the distinct Raman bands [from (1) to (8)] and the spectral profile of the LSPR was obtained for both square and cylinder Au@PNIPAM systems, confirming the strong influence of the near-field spectral profile upon the Raman peak intensities of analytes trapped inside collapsed polymer chains. In these Au@PNIPAM systems, the molecular probes are trapped inside PNIPAM brushes by simple physisorption and are thus distributed all over the polymer layer with no control over their distance from the NP surface. As this is a key parameter for the study of the plasmonic near-field effect on the Raman peak intensities, another functionalization strategy was proposed to improve the control over molecular probe localization inside PNIPAM brushes. It consisted of attaching AB units, at the end of the PNIPAM brushes, by click chemistry. The optical properties of Au@PNIPAM@AB were investigated in water upon heating/cooling cycles (see Figure 7). The LSPR was located at 635 nm in water at 20 °C and slightly shifted to 638 nm after heating above the LCST. The SERS spectra displayed the characteristic Raman lines of AB derivatives with intense Raman bands at ca. 1142 and 1186 cm^{-1} (CN stretching modes), 1414 and 1441 cm^{-1} (ring modes coupled to N=N stretching), 1464 cm^{-1} (N=N stretching), and 1600 cm^{-1} (ring modes: C=C stretching).[30,31] As previously seen, the intensity of all Raman bands was observed to increase with the temperature as shown in Figure 7a. Contrarily, cooling down leads to a decrease of the SERS signal back to its original intensity, as illustrated in Figure S6 with the reversible intensity increase/decrease of the 1142 cm^{-1} band versus temperature. The ratio $I_{40°C/20°C}$ plotted versus the wavelength λ showed a very good correlation with the LSPR of the underlying plasmonic nanostructures with higher enhancement measured when the Raman peaks approach the LSP wavelength (see Figure 7b). This last experiment confirmed that the variations in Raman intensities of molecular probes attached on thermoresponsive brushes reflect the spectral dependence of the near field of the plasmonic structures.

In order to evidence the correlation between the normalized SERS intensities and the plasmon profile, it is important to mention that the plasmonic arrays have been designed here so that their plasmon bands were optimized for the SERS measurements, that is, close to the 633 nm laser line. This is a

DOI: 10.1021/acsomega.8b03107
ACS Omega 2019, 4, 1144−1150

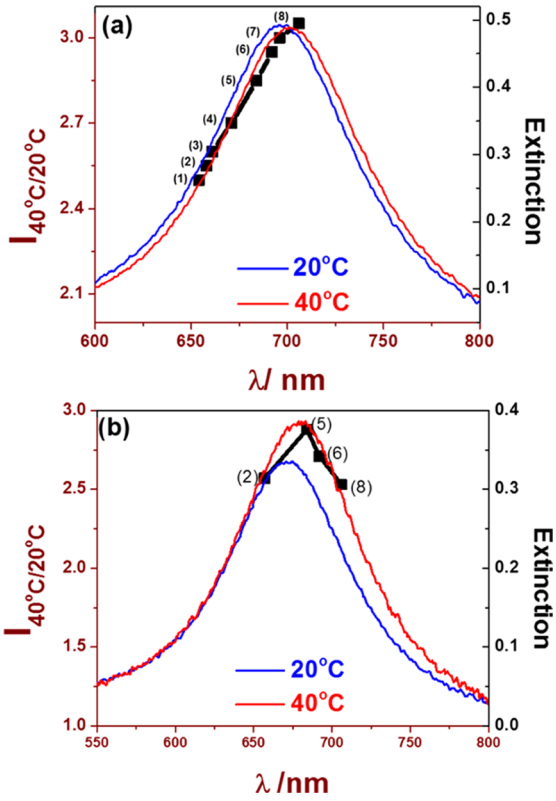

Figure 6. Ratio $I_{40°C/20°C}$ for the various NBA Raman bands (described in Table 1) plotted vs λ and comparison with the extinction spectra of Au@PNIPAM arrays for (a) gold nanosquares and (b) gold nanocylinders.

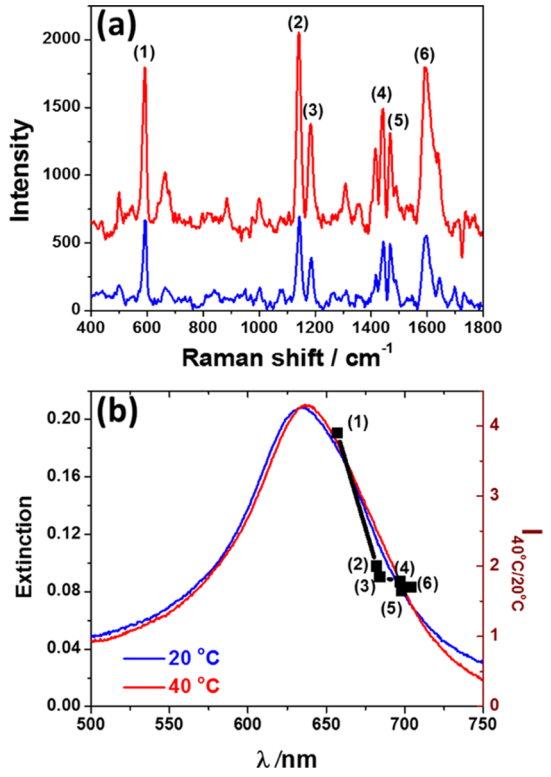

Figure 7. (a) Raman spectra of gold nanocylinder arrays covered by PNIPAM with AB probes at the end chains recorded in water at 20 °C (blue spectrum) and 40 °C (red spectrum). The sample was excited with a 633 nm laser line (6.8 μW), with an acquisition time of 30 s. (b) Ratio $I_{40°C/20°C}$ for the various Raman bands at (1) 592; (2) 1142; (3) 1186; (4) 1441; and (5) 1464 cm^{-1} plotted vs λ and comparison with the extinction spectra of Au@PNIPAM@AB.

necessary condition to detect any molecular probe at a low concentration. However, these SERS experiments could be extended to different laser excitations, by modifying the geometrical parameters of the nanostructures, in order to match the plasmon band with another laser wavelength. In this case, it is expected that the normalized SERS intensities will also qualitatively follow the far-field response of the structures, as these intensities precisely depend on the spectral profile of the plasmon band.

3. CONCLUSIONS

In summary, we have investigated the influence of the spatial and spectral profile of the plasmonic near-field enhancement upon the Raman signal intensity of analytes trapped inside PNIPAM thermoresponsive brushes. For this, well-defined plasmonic arrays (nanosquares and nanocylinders) were modified by PNIPAM brushes using SI-ATRP, resulting in 5−10 nm thick PNIPAM brushes anchored on the NP surface. Molecular probes were trapped inside these Au@PNIPAM nanostructures by simple physisorption or by covalent grafting at the end of PNIPAM brushes, using click chemistry. The optical properties of these plasmonic devices were investigated during heating/cooling cycles, resulting in conformational changes of PNIPAM brushes from a swollen to a collapsed state. The SERS intensity of molecular probes was highly enhanced above the LCST (at 40 °C), when the molecules were located very close to the NP surface, compared to the SERS signals recorded at 20 °C, below the LCST. This behavior was well illustrated by following the ratio $I_{40°C/20°C}$ for the distinct Raman bands as a function of the wavelength λ. Generally, a remarkable correlation was obtained between this ratio and the spectral profile of the LSPR. These results emphasize the strong influence of the near-field spectral profile of the underlying plasmonic nanostructures upon the Raman peak intensities of analytes trapped inside collapsed polymer chains. In other words, the near-field optical response appears to be closely related to the far-field optical response of the NPs. These thermoresponsive plasmonic devices thus provide an ideal dynamic SERS platform to investigate the correlation between the far-field plasmonic profile and SERS response of analytes.

4. EXPERIMENTAL SECTION

4.1. Materials. Reagent grade solvents were purchased from VWR Prolabo and Alfa Aesar. 2-Bromopropionyl bromide (97%, Aldrich), triethylamine (99%, Merck), CuBr (98%, Sigma-Aldrich), *N*,*N*,*N*′,*N*″,*N*″-pentamethyldiethyltriamine (99%, Acros Organics), and NBA (>75%, Sigma-Aldrich) were used as received. *N*-Isoproylacrylamide (99%, Acros Organics) was purified by recrystallization in *n*-hexane solution.

4.2. Functionalization of Gold Nanostructures by PNIPAM Brushes. The gold nanostructures, elaborated by EBL, were functionalized by PNIPAM thermosensitive polymer brushes, following a multistep strategy relying on three major steps: (i) spontaneous grafting of aryl groups derived from 4-hydroxyethylbenzene diazonium tetrafluoroborate salt to produce $-CH_2-CH_2-OH$-terminated aryl

DOI: 10.1021/acsomega.8b03107
ACS Omega 2019, 4, 1144−1150

moieties, covalently anchored to the surface, (ii) esterification of the anchored groups with 2-bromoisobutyryl bromide, and (iii) grafting of PNIPAM brushes via SI-ATRP (see the Supporting Information and Figure S1). The synthesis of diazonium salt is described in the Supporting Information.

4.3. Instrumentation. AFM measurements were performed on a Nanoscope III digital instrument microscope in tapping mode in air. Contact mode AFM was applied in water with a contact SNL-10 silicon tip commercially available from Bruker. Vibration frequency of the tip is chosen at around 7Hz to achieve a stable signal-to-noise ratio in water. AFM images were processed and analyzed using the applications WSxM and FabViewer.[26] The extinction spectra were recorded by far-field extinction microspectroscopy in the 500−1000 nm spectral range. The spectrometer was coupled to an upright optical microscope equipped with 50× (Olympus, numerical aperture NA = 0.35) and 100× (Olympus, NA: 0.8) objectives for experiments in air. Extinction spectra recorded in water at various temperatures used a 100× immersion objective (Olympus, NA: 1). Raman spectra were recorded using a Jobin-Yvon LABRAM HR 800 microspectrometer, using a He−Ne laser excitation (632.8 nm) in backscattering mode. For the experiments in water, the microscope was equipped with a ×100 immersion objective (6.8 μW power). All spectra were recorded within the 400−1800 cm^{-1} spectral range.

■ ASSOCIATED CONTENT

Supporting Information

The Supporting Information is available free of charge on the ACS Publications website at DOI: 10.1021/acsomega.8b03107.

Functionalization strategy of gold nanostructures, AFM images of gold nanostructures before and after functionalization, temperature dependence of the Raman signal of AB on the Au@PNIPAM@AB structures, and details on the FDTD simulations (PDF)

■ AUTHOR INFORMATION

Corresponding Authors

*E-mail: claire.mangeney@parisdescartes.fr (C.M.).
*E-mail: nordin.felidj@univ-paris-diderot.fr (N.F.).

ORCID

Claire Mangeney: 0000-0002-9817-3262

Notes

The authors declare no competing financial interest.

■ ACKNOWLEDGMENTS

M.N. acknowledges the National Foundation for Science and Technology Development (NAFOSTED) for funding support under grant number 103.02-2016.24.

■ REFERENCES

(1) Kneipp, K.; Wang, Y.; Kneipp, H.; Perelman, L. T.; Itzkan, I.; Dasari, R. R.; Feld, M. S. Single Molecule Detection Using Surface-Enhanced Raman Scattering (SERS). *Phys. Rev. Lett.* **1997**, *78*, 1667−1670.

(2) Moskovits, M. Surface-enhanced spectroscopy. *Rev. Mod. Phys.* **1985**, *57*, 783−826.

(3) Fleischmann, M.; Hendra, P. J.; McQuillan, A. J. Raman spectra of pyridine adsorbed at a silver electrode. *Chem. Phys. Lett.* **1974**, *26*, 163−166.

(4) Le Ru, E. C.; Grand, J.; Sow, I.; Somerville, W. R. C.; Etchegoin, P. G.; Treguer-Delapierre, M.; Charron, G.; Félidj, N.; Lévi, G.; Aubard, J. A scheme for detecting every single target molecule with surface-enhanced Raman spectroscopy. *Nano Lett.* **2011**, *11*, 5013−5019.

(5) Nguyen, M.; Kanaev, A.; Sun, X.; Lacaze, E.; Lau-Truong, S.; Lamouri, A.; Aubard, J.; Felidj, N.; Mangeney, C. Tunable Electromagnetic Coupling in Plasmonic Nanostructures Mediated by Thermoresponsive Polymer Brushes. *Langmuir* **2015**, *31*, 12830−12837.

(6) Dieringer, J. A.; McFarland, A. D.; Shah, N. C.; Stuart, D. A.; Whitney, A. V.; Yonzon, C. R.; Young, M. A.; Zhang, X.; Van Duyne, R. P. Introductory Lecture : Surface enhanced Raman spectroscopy: new materials, concepts, characterization tools, and applications. *Faraday Discuss.* **2006**, *132*, 9−26.

(7) Guillot, N.; de la Chapelle, M. L. The electromagnetic effect in surface enhanced Raman scattering: Enhancement optimization using precisely controlled nanostructures. *J. Quant. Spectrosc. Radiat. Transfer* **2012**, *113*, 2321−2333.

(8) Wallace, G. Q.; Pashaee, F.; Hou, R.; Tabatabei, M.; Lagugné-Labarthet, F. Plasmonic nanostructures for enhanced Raman spectroscopy: SERS and TERS of thiolated monolayers. *Proc. SPIE* **2014**, *9126*, 912610.

(9) Le Ru, E. C.; Etchegoin, P. G.; Grand, J.; Félidj, N.; Aubard, J.; Lévi, G.; Hohenau, A.; Krenn, J. R. Surface enhanced Raman spectroscopy on nanolithography-prepared substrates. *Curr. Appl. Phys.* **2008**, *8*, 467−470.

(10) Hao, E.; Schatz, G. C. Electromagnetic fields around silver nanoparticles and dimers. *J Chem Phys* **2004**, *120*, 357−66.

(11) Nguyen, M.; Lamouri, A.; Salameh, C.; Lévi, G.; Grand, J.; Boubekeur-Lecaque, L.; Mangeney, C.; Félidj, N. Plasmon-mediated chemical surface functionalization at the nanoscale. *Nanoscale* **2016**, *8*, 8633−8640.

(12) Nguyen, M.; Kherbouche, I.; Gam-Derouich, S.; Ragheb, I.; Lau-Truong, S.; Lamouri, A.; Lévi, G.; Aubard, J.; Decorse, P.; Félidj, N.; Mangeney, C. Regioselective surface functionalization of lithographically designed gold nanorods by plasmon-mediated reduction of aryl diazonium salts. *Chem. Commun.* **2017**, *53*, 11364−11367.

(13) Winkler, P.; Belitsch, M.; Tischler, A.; Häfele, V.; Ditlbacher, H.; Krenn, J. R.; Hohenau, A.; Nguyen, M.; Félidj, N.; Mangeney, C. Nanoplasmonic heating and sensing to reveal the dynamics of thermoresponsive polymer brushes. *Appl. Phys. Lett.* **2015**, *107*, 141906−141910.

(14) Tijunelyte, I.; Kherbouche, I.; Gam-Derouich, S.; Nguyen, M.; Lidgi-Guigui, N.; de la Chapelle, M. L.; Lamouri, A.; Lévi, G.; Aubard, J.; Chevillot-Biraud, A.; Mangeney, C.; Felidj, N. Multi-functionalization of lithographically designed gold nanodisks by plasmon-mediated reduction of aryl diazonium salts. *Nanoscale Horiz.* **2018**, *3*, 53−57.

(15) Colas, F. J.; Cottat, M.; Gillibert, R.; Guillot, N.; Djaker, N.; Lidgi-Guigui, N.; Toury, T.; Barchiesi, D.; Toma, A.; Di Fabrizio, E.; Gucciardi, P. G.; de la Chapelle, M. L. Red-Shift Effects in Surface Enhanced Raman Spectroscopy: Spectral or Intensity Dependence of the Near-Field? *J. Phys. Chem. C* **2016**, *120*, 13675−13683.

(16) Mosier-Boss, P. Review of SERS Substrates for Chemical Sensing. *Nanomaterials* **2017**, *7*, 142.

(17) Ahmad, R.; Griffete, N.; Lamouri, A.; Felidj, N.; Chehimi, M. M.; Mangeney, C. Nanocomposites of Gold Nanoparticles@ Molecularly Imprinted Polymers: Chemistry, Processing, and Applications in Sensors. *Chem. Mater.* **2015**, *27*, 5464−5478.

(18) Mueller, M.; Tebbe, M.; Andreeva, D. V.; Karg, M.; Alvarez Puebla, R. A.; Pazos Perez, N.; Fery, A. Large-area organization of pNIPAM-coated nanostars as SERS platforms for polycyclic aromatic hydrocarbons sensing in gas phase. *Langmuir* **2012**, *28*, 9168−9173.

(19) Gehan, H.; Fillaud, L.; Chehimi, M. M.; Aubard, J.; Hohenau, A.; Felidj, N.; Mangeney, C. Thermo-induced Electromagnetic Coupling in Gold/Polymer Hybrid Plasmonic Structures Probed by Surface-Enhanced Raman Scattering. *ACS Nano* **2010**, *4*, 6491−6500.

(20) Döring, A.; Birnbaum, W.; Kuckling, D. Responsive hydrogels - structurally and dimensionally optimized smart frameworks for

DOI: 10.1021/acsomega.8b03107
ACS Omega 2019, 4, 1144−1150

applications in catalysis, micro-system technology and material science. *Chem. Soc. Rev.* **2013**, *42*, 7391−7420.
(21) Alvarez-Puebla, R. A.; Liz-Marzán, L. M. Traps and cages for universal SERS detection. *Chem. Soc. Rev.* **2012**, *41*, 43−51.
(22) Pastoriza-Santos, I.; Kinnear, C.; Pérez-Juste, J.; Mulvaney, P.; Liz-Marzán, L. M. Plasmonic polymer nanocomposites. *Nat. Rev. Mater.* **2018**, *3*, 375−391.
(23) Reineke, T. M. Stimuli-Responsive Polymers for Biological Detection and Delivery. *ACS Macro Lett.* **2015**, *5*, 14−18.
(24) Aseyev, V.; Tenhu, H.; Winnik, F. M. Non-ionic Thermoresponsive Polymers in Water. *Adv. Polym. Sci.* **2011**, *242*, 29−89.
(25) Heskins, M.; Guillet, J. E. Solution Properties of Poly(N-isopropylacrylamide). *J. Macromol. Sci., Chem.* **1968**, *2*, 1441−1455.
(26) Horcas, I.; Fernández, R.; Gómez-Rodríguez, J. M.; Colchero, J.; Gómez-Herrero, J.; Baro, A. M. WSXM: a software for scanning probe microscopy and a tool for nanotechnology. *Rev. Sci. Instrum.* **2007**, *78*, 013705.
(27) Nguyen, M.; Sun, X.; Lacaze, E.; Winkler, P. M.; Hohenau, A.; Krenn, J. R.; Bourdillon, C.; Lamouri, A.; Grand, J.; Lévi, G.; Boubekeur-Lecaque, L.; Mangeney, C.; Félidj, N. Engineering Thermoswitchable Lithographic Hybrid Gold Nanorods as Plasmonic Devices for Sensing and Active Plasmonics Applications. *ACS Photonics* **2015**, *2*, 1199−1208.
(28) Gehan, H.; Mangeney, C.; Aubard, J.; Lévi, G.; Hohenau, A.; Krenn, J. R.; Lacaze, E.; Félidj, N. Design and Optical Properties of Active Polymer-Coated Plasmonic Nanostructures. *J. Phys. Chem. Lett.* **2011**, *2*, 926−931.
(29) Álvarez-Puebla, R. A.; Contreras-Cáceres, R.; Pastoriza-Santos, I.; Pérez-Juste, J.; Liz-Marzán, L. M. Au@pNIPAM colloids as molecular traps for surface-enhanced, spectroscopic, ultra-sensitive analysis. *Angew. Chem., Int. Ed.* **2008**, *48*, 138−143.
(30) Jacob, H.; Ulrich, S.; Jung, U.; Lemke, S.; Rusch, T.; Schütt, C.; Petersen, F.; Strunskus, T.; Magnussen, O.; Herges, R.; Tuczek, F. Monitoring the reversible photoisomerization of an azobenzene-functionalized molecular triazatriangulene platform on Au(111) by IRRAS. *Phys. Chem. Chem. Phys.* **2014**, *16*, 22643−22650.
(31) Chaigneau, M.; Picardi, G.; Ossikovski, R. Molecular Arrangement in Self-Assembled Azobenzene-Containing Thiol Monolayers at the Individual Domain Level Studied through Polarized Near-Field Raman Spectroscopy. *Int. J. Mol. Sci.* **2011**, *12*, 1245−1258.

DOI: 10.1021/acsomega.8b03107
ACS Omega 2019, 4, 1144−1150